Pergamon

0301-9322(95)00026-7

Int. J. Multiphase Flow Vol. 21, No. 5, pp. 755–774, 1995

0301-9322/95 $9.50 + 0.00

EXPERIMENTAL INVESTIGATION OF TRANSVERSE FLOW THROUGH ALIGNED CYLINDERS

T. A. K. SADIQ[1], S. G. ADVANI[1]† and R. S. PARNAS[2]

[1]Department of Mechanical Engineering, University of Delaware, Newark, DE 19716, U.S.A.
[2]Polymers Division, National Institute of Standards and Technology, Gaithersburg, MD 20899, U.S.A.

(Received 22 April 1994; in revised form 15 March 1995)

Abstract—In this paper, flow of viscous fluids across an array of solid and porous circular cylinders, which represents a porous media, is explored experimentally. The idealized array or bed of cylinders, which models tows and fibers in a fiber preform used in composites processing, was unidirectional consisting of either solid circular rods or porous circular bundles. By measuring the flow rate and pressure drop across this bed of cylinders, we characterized the transverse permeability of the model porous media. In beds with porous bundles, the volume fraction inside the bundles ranged from 60 to 75% by packing 50–60 nylon fibers into 6.35 mm diameter holes. Both Newtonian and shear thinning fluids were used. These fluids were pumped through the medium such that the flow was perpendicular to the fiber axes. Once the fiber bed was fully saturated, the permeability was determined with the aid of Darcy's law. For the solid rods, the experimental results compare well with the asymptotic model recently developed by Bruschke & Advani for generalized Newtonian fluids. In addition, a heterogeneous fiber bed was constructed, consisting of fiber bundles in a regular array. During the filling stage, the progress of the flow front through the heterogeneous fiber beds was observed and the flow-induced void formation inside the fiber bundles was monitored. None of the existing permeability models could predict the permeability of the heterogeneous porous media. A series expansion was suggested to estimate permeabilities of such heterogeneous media.

Key Words: porous media, permeability, shear thinning fluids, resin transfer molding, composites manufacturing

1. INTRODUCTION

Resin transfer molding (RTM) is a composite manufacturing process that has gained industrial acceptance due to the variety of complex shapes that can be made, the capability of producing closed parts with a core in a single step, good control over mechanical properties, short cycle times and high quality surface finish. Critical processing issues in RTM are the pressure drop and the mold filling time, which are both related to the injection pressure at the inlet. This inlet pressure is a controllable parameter in RTM. If inadequate inlet pressure values are used, the mold will fill very slowly or not at all. Protracted fill time can lead to premature resin cure, leaving unimpregnated preform sections. If excessive pressure is used there may be fiber wash, the cores in the mold may be displaced, and the mold may leak or deform. Hence, the pressure drop experienced across the mold is of great interest, and will depend on the preform permeability to fluid flow. The RTM simulations for fluid flow in complex geometries that have been developed over the past few years require the permeability, or a model for permeability, as input data. This makes the permeability of a preform to fluid flow, or the flow mobility, an important consideration in the design of an RTM process (Bruschke & Advani 1992; Johnson 1987; Bruschke 1992; Advani *et al.* 1994) and the permeability has been shown to be closely related to the preform structure (Parnas & Salem 1993).

Fibrous preforms are modeled as porous media, and their structures are often characterized by three parameters: (1) average fiber radius (R_f), (2) volume fraction of fibers (v_f); and (3) the orientation of the fibers. The ratio of volume filled by the fibers to the total volume defines the fiber volume fraction. If all the fibers are assumed to span the entire mold, have the same

†To whom correspondence should be addressed.

radius, and are uniformly spaced, this ratio is defined by the fiber radius and their center spacing (C_s):

$$v_f = \frac{\pi R_f^2}{C_s^2} \quad [1]$$

This definition is conceptually equivalent to a definition based on the mass of the preform, the mold volume and the fiber density. Thus, the conventional method for calculating volume fraction is really an "averaged" volume fraction over the entire mold. However, preform fiber mats often consist of fiber tows, or groups of bundled fibers. This bundling occurs due to the difficulty in handling individual fibers. Tows are woven (or braided) into a fabric and preformed to the shape desired before resin impregnation. While fiber tows make the fibers easier to handle, they introduce additional processing complexities. The reinforcement structure becomes heterogeneous with a broad range of local volume fractions. For example, the volume fraction inside a fiber tow is much higher than the volume fraction outside the tow. The "averaged" volume fraction derived by weighing the preform or using [1] falls somewhere between the volume fractions inside and outside the tow. As the flow spreads through the mat, it may flow preferentially around the tows in the regions of higher permeability, rather than through the inner portion of the tow. That resin flow pattern can trap air inside the tow, and thus cause void formation inside the tow (Parnas & Phelan 1991; Sadiq *et al.* 1992). After fabrication, if a composite part has voids in excess of 1% of its volume, performance can be significantly reduced (Broutman & Krockl 1967; Agarwal & Broutman 1980; Grove 1980). For example, moisture absorption can increase and fatigue properties decrease as void fraction increases.

A number of current research activities are focused on modeling the permeability based on the preform structure. While these efforts are currently limited to flows parallel or transverse to unidirectional arrays of ellipsoids, it is worth verifying such models before more complex geometries are simulated. Previous attempts at model verification have had mixed results, and experimental uncertainties due to structural heterogeneities in the unidirectional mats have been hypothesized to be the cause. Both to avoid and to assess the effects of heterogeneity on the permeability measurement, model porous media were constructed for this study.

The three goals of this paper are: (1) to experimentally verify the asymptotic model of flow through porous media by measuring the permeability in a porous media composed of an ideal array of cylinders, (2) to demonstrate the effects of structural heterogeneity on the flow behavior and (3) to determine the effects of fluid rheology on permeability. Other fluid flow issues, including surface tension of fluids, surface effects and wetting of the porous media, will not be addressed here. Although research has shown these other parameters may influence some types of permeability measurement, it has also been shown that these effects are minor when compared to the effect of the porous media structure. Experimental results will be compared to the recently developed asymptotic model of permeability by Brushke & Advani (1992). The micro-level effects due to heterogeneity in the fibrous porous media observed in the fiber bundle experiments, and the qualitative description of voids and their effects on overall bed permeability will also be discussed.

2. MODELS FOR FLOW TRANSVERSE TO ALIGNED FIBERS

Darcy's law (Darcy 1856) is a commonly accepted model for flow through porous media, including the fibrous materials used for structural composite reinforcements (Johnson 1987; Brown 1984). The one-dimensional form of Darcy's law relates the flow rate, Q, to the pressure gradient, $\mathrm{d}\mathbf{P}/\mathrm{d}x$, in the direction of flow,

$$Q = \frac{KA}{\mu}\frac{\mathrm{d}\mathbf{P}}{\mathrm{d}x} \quad [2]$$

where μ is the viscosity, A is the cross-sectional area and the proportionality constant, K, is called the Darcy permeability. Q/A can also be regarded as the momentum flux or superficial velocity of the fluid. Darcy's law was developed for the flow of fluids through beds of particles and has been generalized to multiple dimensions where one relates the velocity field to the gradient of the pressure by expressing the permeability as a second order tensor. In this paper we need only consider the one-dimensional form of Darcy's equation.

The capillary model

The permeability has generally been shown to decrease sharply as the volume fraction of the obstructions increase. Many analytical solutions, including capillary models, express the permeability in dimensionless terms of K/r^2, where r is the average radius of the constituent particles in the porous media. For review, see Skartsis *et al.* (1992). Figure 1 shows this dependency as modeled by the Kozeny–Carman (Carman 1937) equation and by the recently developed asymptotic model of Bruschke & Advani (1992). Kozeny (1927) used the capillary model to relate the pressure drop to velocity. He developed his expression by assuming flow through an idealized, isotropic (i.e. random, granular), porous media consisting of tortuous capillaries. The concept of the hydraulic radius was used to relate the dimensions of the capillary to the parameters of the porous media. Carman (1937) modified this equation by incorporating the specific surface area of the porous media particles. The Kozeny–Carman equation expresses the permeability as a function of volume fraction, particle radius and the Kozeny–Carman constant, $K_0K_1^2$, as shown below:

$$K = \frac{r^2}{(9K_0K_1^2)} \frac{(1-v_f)^3}{(v)^2} \quad [3]$$

It is interesting to note that the Kozeny–Carman equation applies only to one-dimensional flows and the permeability is expressed as a scalar quantity. There is no straightforward way to generalize it to multiple dimensions. In the Kozeny–Carman constant $K_0K_1^2$, K_0 is a geometric shape factor that accounts for the difference in shape of the particles of a porous media while other parameters are equal. The factor K_1 is the tortuosity.

The capillary model that Carman & Kozeny developed to describe the flow of viscous fluids through porous media is based on an isotropic bed of spheres. Experimental investigation of such beds has shown good agreement with this model (Aström *et al.* 1992). The adaptation of the capillary model to the highly anisotropic case of flow across an aligned (unidirectional) fiber bed was achieved only by redefining the hydraulic radius (Williams *et al.* 1974; Lam & Kardos 1989).

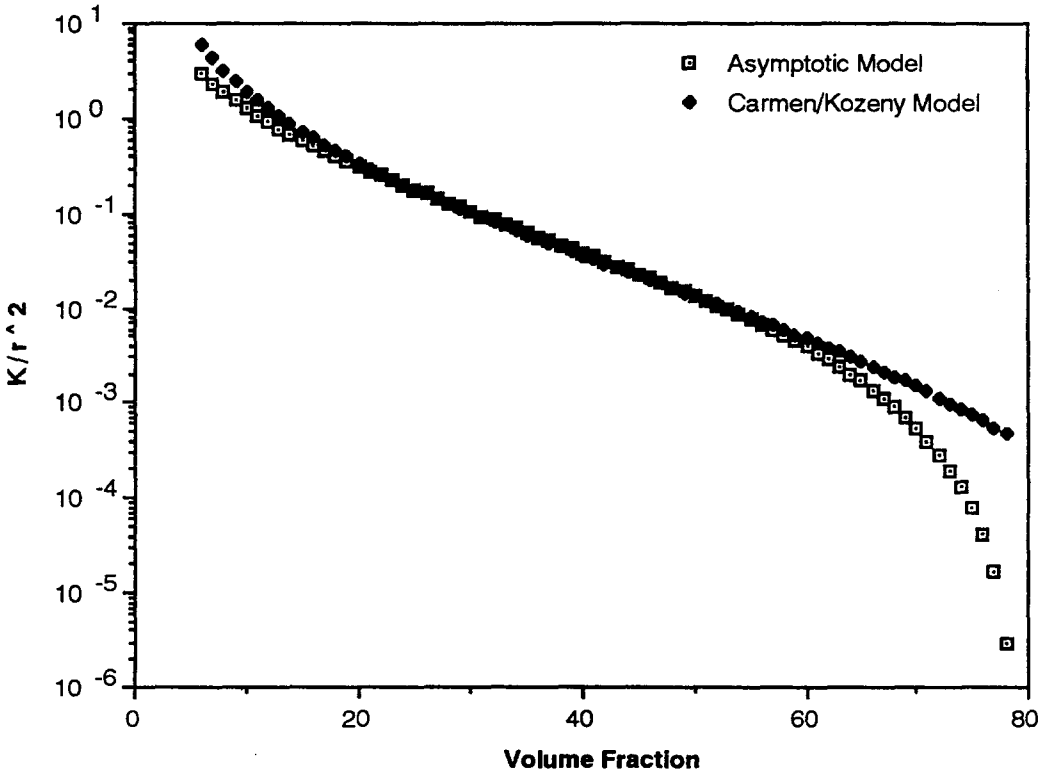

Figure 1. (K/r^2) vs volume fraction as predicted by the asymptotic and the Kozeny–Carman models.

Since the geometry of the flow channel was not addressed, experimental agreement has not been very consistent with this model. Researchers often compensate for this discrepancy by adjusting the Kozeny–Carman constant to fit the data, but the Kozeny–Carman constant should in fact be constant for a given geometry. Some researchers have found the Kozeny–Carman constant to increase with volume fraction, while others have found it to decrease (Aström *et al.* 1992; Williams *et al.* 1974; Gutowski *et al.* 1987; Skartsis & Kardos 1990). Some have found fluid dependence; others have found none (Aström *et al.* 1992; Williams *et al.* 1974; Gutowski *et al.* 1987). Due to this scatter, no specific conclusions are drawn about the validity of a predictive model for permeability based on the capillary approach.

Recently, however, Bruschke & Advani (1992) showed that due to inherent assumptions in the capillary model, it is not a suitable choice to predict the flow across a fiber bed. They performed numerical calculations of creeping flow around cylinders and determined the values of the Kozeny–Carman constant. The results indicate that, contrary to the Kozeny–Carman equation, $K_0K_1^2$ is not a constant. Differences of up to an order of magnitude exist between permeability results from the capillary model and results from numerical models.

The asymptotic model

A large difference between the capillary and asymptotic models appears at high volume fractions in figure 1, and this difference points out why the capillary model is inappropriate for use with porous media containing arrays of aligned fibers. Note that the Carmen–Kozeny model, [3], predicts a zero value of the permeability at a value of $v_f = 1$. However, an array of cylinders reaches a maximum packing fraction at $v_f < 1$ (~ 0.78 for a square array), at which the transverse permeability goes to zero. Thus, the Carmen–Kozeny model is expected to overpredict the permeability, especially at high volume fractions.

A more credible approach than the capillary model for predicting the permeability would be to idealize an aligned fiber bed as an array of regularly spaced cylinders (Sangani & Acrivos 1982; Bruschke & Advani 1992; Chmielewski *et al.* 1990). Solving the Stokes flow equations in such a model geometry would render unnecessary the approximations of hydraulic radius, tortuosity and shape factor. The complex geometry of regular arrays of cylinders cannot be solved exactly in closed form for the flow over the full range of possible volume fractions (5–78% in the case of square arrays). However, analytical solutions for the aligned fiber bed geometry at very high and very low volume fractions are possible (Bruschke 1992). At high volume fractions, the lubrication approximation can be used to solve for the flow through the array. At low volume fractions, the cell model can be used to determine the flow through the array. Once the flow is derived from the model, the permeability can be obtained from Darcy's law. An asymptotic matching procedure can then be used to obtain a closed form solution of the permeability over the entire volume fraction range, hence the name asymptotic model. The entire model can also be extended to address generalized Newtonian fluids.

The relationship of the flow rate to the pressure drop for Newtonian fluids, in the cell model, yields the dimensionless permeability for low fiber volume fractions:

$$\frac{K}{r^2} = \frac{l_c^2}{4}\left(\ln(l_c) - \tfrac{3}{4} + l_c^{-2} - \frac{l_c^4}{4}\right) \qquad [4]$$

where l_c is the ratio of the cylinder radius to the cell radius and is related to volume fraction by

$$l_c^2 = \frac{1}{v_f} \qquad [5]$$

The relation between flow rate and pressure drop in the lubrication approximation allows one to establish the dimensionless permeability for high volume fractions:

$$\frac{K}{r^2} = \frac{1}{3}\frac{(1-l_n^2)^2}{l_n^3}\left(3l_n\frac{\arctan\left(\sqrt{\dfrac{1+l_n}{1-l_n}}\right)}{\sqrt{1-l_n^2}} + \frac{1}{2}l_n^2 + 1\right)^{-1} \qquad [6]$$

where l_n is the ratio of half the center spacing divided by the cylinder radius and is related to volume fraction as

$$l_n^2 = \frac{4}{\pi} v_f \quad [7]$$

Bruschke & Advani (1992) used an asymptotic matching function to combine the solutions from the lubrication approximation and the unit cell model. The resulting formulation is a solution that is valid across the entire volume fraction range and agrees very well with the numerical calculations of flow across an idealized array of cylinders. Note that at high volume fractions, figure 1 shows that the asymptotic model predicts much lower values of the permeability than does the capillary model.

The micro-flow model

In addition to the macroscopic flow behavior described above, small scale flow behavior may occur that is important to the performance of composite parts manufactured by liquid molding. For example, voids may form at the flow front due to non-uniformities in the reinforcement which lead to the creation of preferential flow pathways (Parnas & Phelan 1991; Haywood & Harris 1990; Parnas *et al.* 1994). In such cases, the macroscopic flow may be modified as well as the final part properties.

A one-dimensional model of behavior at the flow front has been presented for the case under discussion, namely transverse flow through heterogeneous structures of aligned fibers (Parnas & Phelan 1991), and will be briefly summarized here. In an RTM process, a preform may contain fibers oriented in many directions, and fluid flow may occur in several directions relative to the fibers. Rather than beginning with the analysis of such a complex case, the simplified geometry depicted in figure 2 is used as a first-order model for demonstrating the effect of fiber impregnation. The model geometry shows a unidirectional flow perpendicular to the fiber bundles. It is assumed that as the advancing flow front encounters a fiber bundle, it flows around it, entrapping a pocket of air as it does so. After the front surrounds and bypasses a fiber bundle, the fiber bundle is slowly impregnated with fluid but may not completely fill. The basis for the assumed entrapment mechanism is that the interstitial spaces within the fiber bundles are much smaller than the spaces between the fiber bundles that make up the preform. Thus, it is expected that the permeability of a fiber bundle to resin impregnation is much less than the permeability of the preform to resin flow.

To quantify the effects of the impregnation process on the advance of the flow front, the fiber bundles are treated as flow sinks which remove fluid from the flow advancing through the preform. A mass balance on a slice of the preform of a size appropriate for volume averaging the

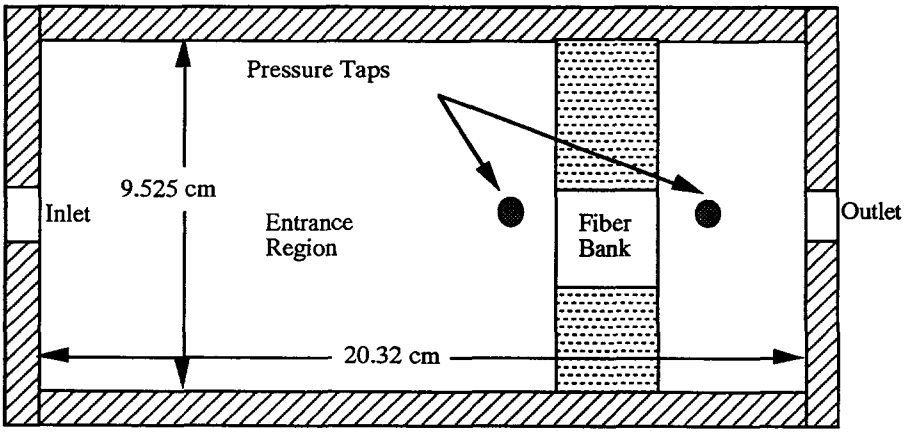

Figure 2. Experimental mold.

macroscopic flow yields a relationship between the fluid velocity V and the rapidity of the impregnation process

$$\frac{dV}{dx} = \frac{q(x,t)}{C_s^2} \quad [8]$$

where $q(x,t)$ is the sink strength at position x in the mold at time t. Equation [8] has a very simple interpretation. For $q < 0$ (note that $q < 0$ for a fluid sink), the impregnation process of the fiber bundles causes a reduction in the superficial fluid velocity as the front penetrates further into the preform, for as long as the sinks are active. When $q = 0$ (i.e. impermeable fiber bundles or inactive sinks) then $dV/dx = 0$ and the fluid velocity in the preform is uniform for the simple unidirectional flow problem considered here. Note also that [8] is the equation of continuity, and that macroscopic flow simulators based on Darcy's law all solve the flow equations assuming the continuity equation to be homogeneous, i.e. $\nabla \cdot V = 0$. This model for flow in heterogeneous porous media couples the flows at different length scales by making the continuity equation inhomogeneous at the macroscopic length scale.

The Darcy law model and continuity equation for the macroscopic flow cannot be solved until a specific expression for the sink strength q is specified. Such an expression is obtained by considering the microscopic flow of resin into the fiber bundle. Darcy's law for radial flow is used to relate the radial fluid velocity and the radial pressure gradient, dp/dr, within the fiber bundle. Solving the model for radial flow into the fiber bundles is complicated by the fact that the radial pressure gradient is not constant, but must be expressed as

$$\frac{dp}{dr} = \frac{p_0 R_f^2/\mathscr{R}^2 - p_\infty}{r \ln\left(\frac{\mathscr{R}}{R_f}\right)} \quad [9]$$

where $\mathscr{R}$ is the radial position of the front penetrating the fiber bundle at time t, R_f is the fiber bundle radius, p_0 is the initial pressure in the mold before the filling operation began and p_∞ is the pressure outside the fiber bundle at time t. The term $p_0 R_f^2/\mathscr{R}^2$ in [9] arises from the internal pressure in the fiber bundle which increases as the radial fluid position, $\mathscr{R}$, decreases (due to a decrease in gas volume in the fiber bundle). The pressure outside the fiber bundle, p_∞, varies with time due to the global flow outside the fibers.

The rate of penetration of the fluid into the fiber bundle is found by substituting [9] into Darcy's law for radial flow and evaluating the fluid velocity at $r = \mathscr{R}$; this yields

$$\frac{d\mathscr{R}}{dt} = \frac{\kappa p_0 R_f^2/\mathscr{R}^2 - p_\infty}{\mu \mathscr{R} \ln\left(\frac{\mathscr{R}}{R_f}\right)} \quad [10]$$

where κ is the permeability within a fiber bundle. This last expression enables the determination of the desired quantity, the sink strength q, via the relation

$$q(x,t) = 2\pi \mathscr{R} \frac{d\mathscr{R}}{dt} \quad [11]$$

and the sink strength, q, couples the penetration of the resin into the fiber bundles with the flow in the preform outside the fiber bundles. Equations [10]–[11] indicate that after the flow front engulfs a fiber bundle the sink strength of the fiber bundle increases due to an increase in p_∞, the pressure of the fluid outside the fiber bundle. As the sink strength increases, fluid is removed from the advancing flow into the fiber bundle, thus simulating the impregnation process. The sink strength approaches zero at a later point in time when the pressure inside the fiber bundle comes into equilibrium with the pressure outside the fiber bundle.

The microflow phenomena described above have consequences on the macroscopic flow, both during the initial mold filling and on the steady state flow after the mold is filled. The effect of the microflow on the steady state macroflow can be assessed with permeability measurements. Assessing the effect of the microflow on the transient mold filling behavior requires more detailed observations.

3. EXPERIMENTAL

The approach in the current experiments was, first, to force a Newtonian fluid to flow through a porous media consisting of homogeneous arrays of circular, rigid fibers oriented perpendicular to the direction of flow. The pressure drop across the media and the flow rate through the media were measured. The Darcy permeability was calculated from these values with [2]. Since the pressure drop across a preform is dominated by the flow transverse to the fibers, this quantity is very important in characterizing preform permeability. The volume fraction range significant for typical fiber composites, from 40 to 60%, was investigated. Two different fiber radii, 0.0794 cm aluminum welding rods and 0.3175 cm nylon stock, were used to determine the validity of the claim of the various models that the dimensionless value of K/R_f^2 is only a function of the volume fraction of a homogeneous porous media.

In a second set of experiments, a model heterogeneous porous media was constructed to determine the effect of preform heterogeneity on permeability. In this experiment, the 0.3175 cm radius solid nylon rods used in the aforementioned experiment were replaced by fiber bundles, simulating the reinforcing fiber tows in composites. These fiber bundles consisted of numerous 0.07112 cm diameter nylon fibers inserted into 0.635 cm diameter holes. the 0.635 cm bundles were placed in an array at volume fractions of 40 and 50%. The volume fraction of 0.07112 cm fibers inside the bundle was varied from 62 to 75% by inserting different numbers of 0.07112 cm fibers into the 0.635 cm holes. This type of bed more closely resembles a true fiber preform than do the beds made of homogeneous arrays of cylinders used in previous investigations (Chmielewski *et al.* 1990). Void formation inside the fiber bundles was observed, and the permeability of the model heterogeneous porous media was measured. Care was taken to completely saturate the model fiber tows with fluid before the permeability of the heterogeneous porous media was measured.

A third set of experiments was conducted to characterize the flow of shear thinning fluids in the model arrays of cylinders. Although a great deal of experimental work has focused on flow of shear thinning fluids in particulate porous media, little experimental research has been published in the area of flow of shear thinning fluids transverse to fiber beds (Chmielewski *et al.* 1990). The analysis of shear thinning flow is more difficult than for Newtonian flow because viscosity varies with shear rate.

Although most models assume homogeneous arrays of rigid circular fibers, most previous research has been conducted on real fiber beds, and there has been little experimental work done on homogeneous arrays of rigid circular fibers (Williams *et al.* 1974; Skartsis & Kardos 1990; Gebart 1990). This is due to the difficulty of constructing ideal fiber beds. Thus, it is difficult to experimentally evaluate the validity of such models, as all the researchers attribute the discrepancies in their results to heterogeneities in the porous media, fiber waviness, voids and other inconsistencies due to the nature of real fiber beds. Experiments were conducted on idealized fiber beds to eliminate these perturbations. Bruschke's (1992) asymptotic model was extended to describe the flow of shear thinning fluids, and the experimental results for a well characterized fluid will be compared with that model.

Experimental materials

All experiments were conducted with square arrays of cylinders or fiber bundles. The idealized fiber beds were constructed using acrylic plates with drilled holes spaced in a square array, where the center spacing was defined by the volume fraction and size of fiber of the fiber bed (see [1]), as illustrated in figure 3. Twelve rows of fibers were used to form the fiber beds, with fibers spanning the channel width of 9.525 cm. One experiment was also conducted with 4 rows of fibers, the results were nearly identical to the corresponding experiment conducted with 12 rows, indicating that the flow field develops quickly within the fiber beds and that twelve rows of fibers were sufficient for the experiments. The number of rods placed across the channel varied with volume fraction and rod radius from 11 (40% v_f with 0.3175 cm rods) to 56 (60% v_f with 0.079375 cm rods). The channel length of 20.32 cm was used to ensure that the flow was fully developed through the majority of the media. The channel depth was 1.905 cm. Since the top and bottom plates were clear acrylic, the flow could be visually inspected to detect any flow irregularities, such as edge effects, clogging

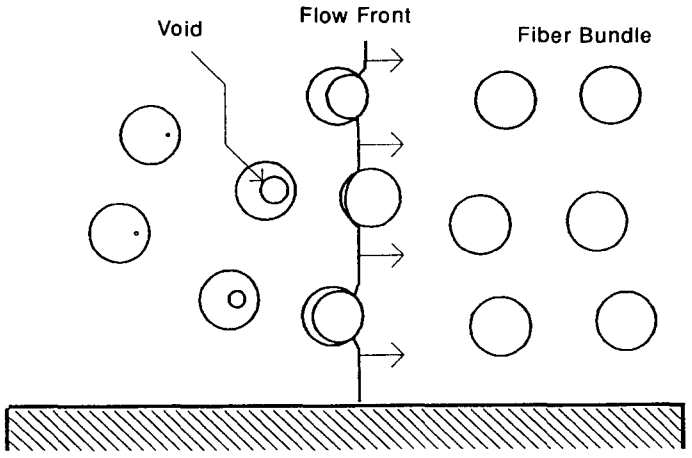

Figure 3. Void entrapment in heterogeneous porous media.

or stagnation. Fluid pressure in the mold was never large enough to cause deflection of the acrylic sides.

Both solid fibers and fiber bundles were used in the experiments. The fiber bundles greatly increase the flow complexity and the architecture of aligned arrays of cylinders. Hence, a new nomenclature that clarifies this heterogeneous porous media is introduced. Nominal volume fraction (N_{vf}) refers to the volume fraction of the fiber bed as if the resident fibers, of radius R_f, were solid. This volume fraction describes the homogeneous porous media composed of solid rods. Tow volume fraction (T_{vf}) refers to the volume fraction of the fibers inside each fiber bundle of radius R_f. The T_{vf} is based on the area taken by a number (N) of fibers of radius R_b divided by the area of the hole of radius R_f. Global volume fraction (G_{vf}) is the volume fraction that would exist if the small fibers of radius R_b were distributed homogeneously in the fiber bed, and G_{vf} is the quantity that would be obtained from the weight, density and volume occupied by the porous media. This is the volume fraction that would exist if the heterogeneous fiber bed was homogeneous with resident fibers of radius R_b. Effective cylindrical volume fraction (C_{vf}) refers to the volume fraction that would exist if all the fibers inside a bundle were combined into one solid fiber of radius R_c. The fiber radius, R_c, equals the square root of the number of fibers in the tow times R_b^2 as shown in [12e]. Thus, R_c is used to determine the effective cylindrical volume fraction, C_{vf}. The center spacing remains the same as that for the solid fiber bed. These relationships are described mathematically as follows:

$$N_{vf} = \frac{\pi (R_f)^2}{C_s^2} \quad [12a]$$

$$T_{vf} = N\left(\frac{R_b}{R_f}\right)^2 \quad [12b]$$

$$G_{vf} = \frac{NN_T\pi (R_b)^2}{A} \quad [12c]$$

$$C_{vf} = \frac{N\pi (R_c)^2}{C_s^2} \quad [12d]$$

$$R_c = \sqrt{N(R_b)^2} \quad [12e]$$

where the total area of the porous bed is denoted by A, the center spacing between holes with radius R_f is denoted by C_s and the total number of tows with radius R_f is given by N_T and is equal to the number of holes drilled to construct the fiber bed. Table 1 provides the parameters used in the experiments conducted with fiber bundles.

Two fluids were used for the experiments. Corn syrup was used as the model Newtonian fluid. Viscosity tests over a wide range of shear rates indicated that the corn syrup was not strictly

Table 1. Fiber bundle parameters

N_{vf} (%)	T_{vf} (%)	G_{vf} (%)	C_{vf} (%)	N	R_f (cm)	R_b (cm)	R_c (cm)
50	75.3	38.38	37.64	60	0.3175	0.0356	0.275
40	69.0	29.05	27.58	55	0.3175	0.0356	0.264
40	62.7	26.40	25.09	50	0.3175	0.0356	0.251

Newtonian, but had a power law index of $n = 0.99$. This is regarded as being close enough to a Newtonian fluid for the purposes of these experiments. The viscosity ranged from 4.9 to 10 Pa s. Viscosity and density were measured before and after each trial, and no significant changes were detected.

The second fluid used was a solution of Carbopol, a polymer manufactured by B.F. Goodrich. The Carbopol was mixed into distilled water at 5% concentration by weight. Sodium hydroxide, 0.025% by weight, was added to the mixture to neutralize it. Additional water was added to dilute the Carbopol solutions to the desired consistency. Water thinned the Carbopol and changed the shear index. Carbopol exhibits shear thinning behavior and can be characterized as a generalized Newtonian fluid by using the power law model, [13], which relates shear rate, $\dot{\gamma}_{xy}$, to shear stress, τ_{xy}:

$$\tau_{xy} = \mu(\dot{\gamma}_{xy}) \quad [13a]$$

$$\mu(\dot{\gamma}_{xy}) = m|\dot{\gamma}_{xy}|^{n-1} \quad [13b]$$

where n is the shear index and m is the consistency index. A Brookfield viscometer was used to characterize the fluid before and after each experiment. Characterizations performed on the same fluid at different times produced nearly identical results. A characteristic of this fluid that complicated the experiments was that it demonstrated an apparent yield stress, especially in the more concentrated solutions of Carbopol. However, dilute solutions provided insufficient pressure drop across the fiber bed to accurately measure the permeability. A compromise was found where the yield stress appeared insignificant and the pressure drops generated in the experiments could be accurately measured. For those cases, the Carbopol concentration was adjusted to produce a solution with a consistency index of approximately 25 Pa s (250 poise).

Experiments were carried out with the Carbopol solutions flowing in the arrays of the 0.0794 cm radius aluminum welding rods, and the rheology of the fluid used in each experiment is summarized in table 2. The rheological parameters given for the Carbopol solution used in the experiment at a 50% volume fraction have a rather large range because that sample of Carbopol was the first one characterized, and the characterization data were not completed properly. Experiments with the Carbopol in the arrays of nylon rods are not reported because the fluid did not appear to wet the rods well and consistent results could not be obtained.

The fluids were driven through the mold transverse to the rods via a gas drive pump. This pump consists of a large stainless steel tank with an outlet at the bottom. Pressurized gas was injected from the top of the tank, which drove the fluid out of the bottom of the tank at a constant pressure. Once the fiber bed was saturated, the flow rate remained constant as long as the tank pressure was constant. This pump created and allowed for long term steady flow through the apparatus. The flow was easily controlled by varying the inlet pressure from a regulator on the nitrogen tank. The pressure drop was recorded across the bed of fibers. Flow was measured at the outlet. From these values, the Darcy permeability was computed. The pressure drop across the fiber bed was measured by an inverted U-tube manometer or a 17.24 MPa (2.5 psi) differential pressure transducer.

Table 2. Rheological characterization of Carbopol solutions pumped through arrays of 0.0794 cm radius aluminum welding rods

N_{vf} (%)	Shear index, n	Consistency, m (Pa s)
40	0.44	23.1
50	0.39–0.54	27.7–29.7
60	0.40	28.8

Table 3. Permeability for 0.635 cm diameter nylon rods

N_{vf} (%)	Error in N_{vf}, ±%	Experimental K	Experimental error (%)		Bruschke K (cm^2)	Percent difference
40.8	0.3	3.90×10^{-3}	−10.36	+8.54	3.51×10^{-3}	11.14
51	0.4	1.23×10^{-3}	−3.41	+10.12	1.20×10^{-3}	2.19
61.2	0.5	3.02×10^{-4}	−8.10	+7.80	3.23×10^{-4}	−6.5

The permeability of the heterogeneous fiber bundles was measured in a similar fashion. In additon to the permeability measurements, the transient mold filling flow at the microscopic scale was recorded onto video tape. The contrast of the fluid and the nylon fibers was enhanced by adding red food coloring to the corn syrup.

4. RESULTS

Results with corn syrup and solid rods

A range of experiments was carried out with a Newtonian fluid and homogeneous porous media to give a good basis by which to judge the asymptotic model of Bruschke (1992). Three nominal volume fractions, 40, 50 and 60%, were used with two different fiber radii. The data collected from these experiments were reduced to yield a permeability, and excellent agreement with the model was obtained. Tables 3 and 4 show the experimentally derived permeability results tabulated with the permeability predictions of Bruschke's asymptotic model. The experimental permeability was obtained from the slope of a least-squares fit line of fluid velocity, V, plotted against the ratio of pressure gradient to viscosity ($\nabla P/\mu$). The errors in nominal fiber volume fraction, N_{vf}, were calculated from the standard deviation of the measured diameter of several hundred fibers. The errors in the permeability were computed by error propagation from expected errors in pressure, flow rate and viscosity values. Agreement is very good in all cases, and within 7% for all but one case. The 11% deviation in the test conducted with the 0.635 cm diameter rods at an N_{vf} of 40.8% is believed to be due to non-systematic experimental errors. This test was one of the first experiments conducted. Figure 4 illustrates the results with a plot of $\log K/R_f^2$ vs volume fraction using the experimentally obtained values for the two rod sizes and the values predicted by Bruschke's asymptotic model. Although the range of fiber radii tested was small, figure 4 indicates that the dimensionless ratio K/R_f^2 appears to be a valid scaling of the permeability. The agreement of the experimental results with both Bruschke's model and numerical calculations indicates that the experimental setup and design was valid for flow regimes transverse to aligned fibers.

Results with Carbopol and solid rods

The results for the experiments with a shear thinning fluid are presented in terms of the flow mobility. The flow mobility, M, for a shear thinning fluid is analogous to K/μ for the Newtonian case (see [2]). Therefore, for shear thinning fluids, M is expected to vary with the pressure gradient since the fluid viscosity changes with shear rate, unlike the case of a Newtonian fluid where the ratio K/μ is a constant. Experimentally M can be expressed simply as the ratio of the superficial fluid velocity to the pressure gradient. A log–log plot of M vs ∇P should be linear with a slope of $(1/n) - 1$, reflecting the power-law dependence of the viscosity on the pressure gradient. Perturbation of the consistency index, m, shifts the graph vertically but does not affect the slope. For the Newtonian case, $n = 1$ and $M = K/\mu$ is a constant with no dependence on pressure gradient.

Figures 5(a)–(c) show the experimentally determined values of the flow mobility, as well as the results computed by the asymptotic model and the Newtonian solution, for the three cases where

Table 4. Permeability for 0.1588 cm diameter aluminum rods

N_{vf} (%)	Error in N_{vf}, ±%	Experimental K (cm^2)	Experimental error (%)		Bruschke K (cm^2)	Percent difference
38.9	1.3	2.51×10^{-4}	−10.10	+5.83	2.66×10^{-4}	−5.60
48.6	1.7	9.79×10^{-5}	−8.8	+7.29	9.78×10^{-5}	0.07
58.3	2.0	3.28×10^{-5}	−9.10	+7.94	3.08×10^{-5}	6.62

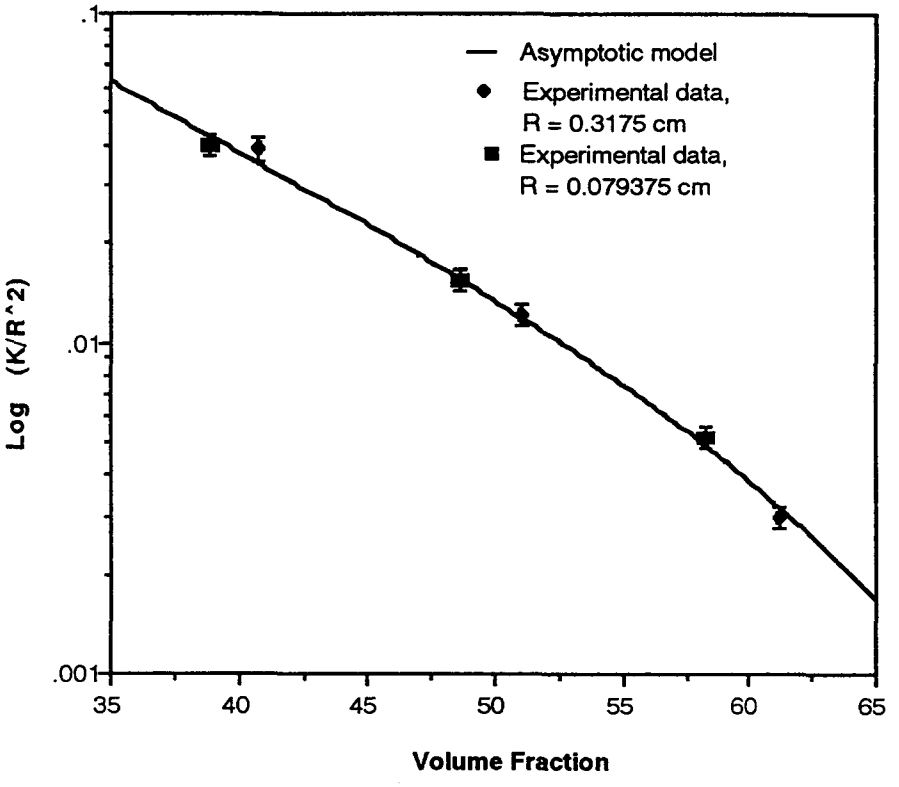

Figure 4. Log K/r^2 vs volume fraction for the experimental data collected in square arrays of cylinders.

Carbopol solutions were pumped through arrays of 0.1588 cm diameter aluminum welding rods. The solid line through the experimental points in each figure is a least squares fit of the data. The slope of the least squares fit line can be used to compute the apparent shear index n of the fluid in the porous media for comparison to the value of n determined during the fluid characterization measurements (see table 5). The fluid flow behavior in the porous media is clearly consistent with the rheological characterization data. While additional calculations could render the results in terms of shear stress and shear rate for comparison to the power-law model, that is not necessary because of the detailed comparison between the experimental results and the asymptotic model also shown in figures 5(a)–(c).

A comparison of the experimental results with the asymptotic model demonstrates that the flow behavior of power-law fluids in arrays of cylinders can be predicted from the porous media structure, albeit not as accurately as the flow of Newtonian fluids. It is important to note that the model calculations used the fluid rheological constants measured in the Brookfield viscometer to provide results independently of the porous media experiments. The two "model" lines in figure 5(b) bracket the experimental data, and were computed for two values of the shear index, $n = 0.39$ and $n = 0.54$, because the original characterization of that batch of Carbopol solution was accurate only to that tolerance (see table 2). The vertical offset between the experimental data and the model calculations may arise from inaccuracies in either the characterization of the consistency index, m, or from errors in the measurement of pressure. Also, the small yield stress of the fluid remaining after the Carbopol concentration was optimized for these experiments may have contributed to the discrepancies between experiment and model calculation. Nevertheless, the model calculations of flow mobility are within roughly 30% of the experimental values.

Results with fiber bundles and corn syrup

Several tests were conducted with bundles of 0.07112 cm diameter fibers inserted into the 0.635 cm diameter holes in place of 0.635 cm diameter solid rods. These tests demonstrated the

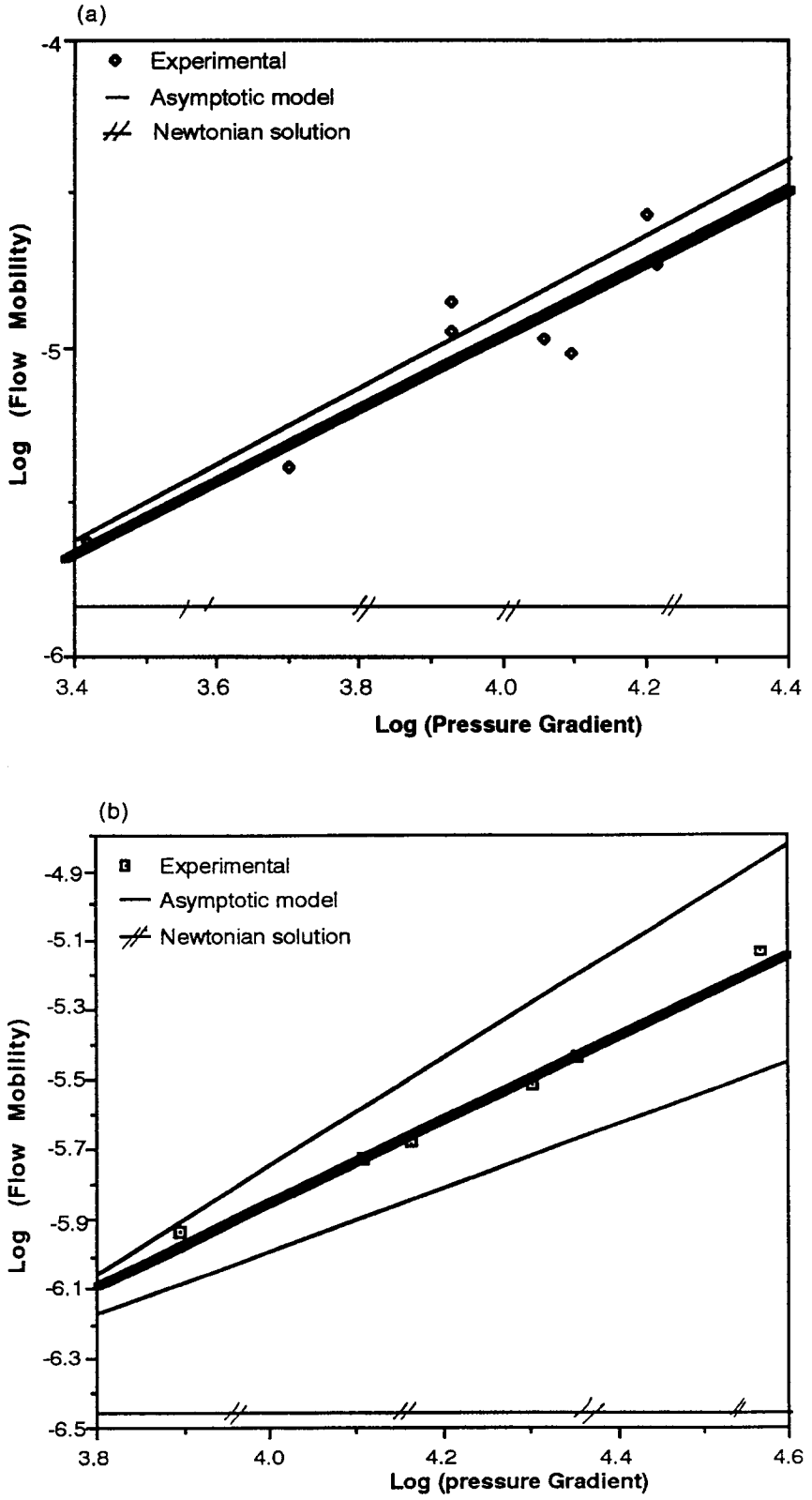

Fig. 5(a) and (b). *Caption on facing page.*

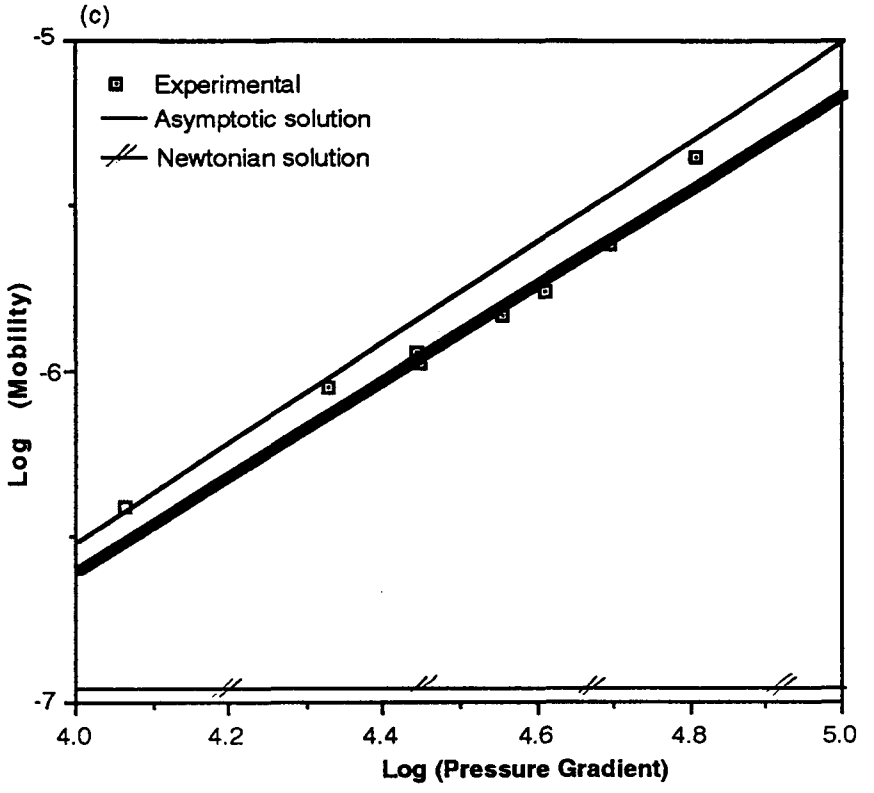

Figure 5(c).

Figure 5. The flow mobility vs pressure gradient for the flow of shear thinning fluids in arrays of 0.073 cm radius aluminum welding rods. (a) 40% nominal volume fraction; (b) 50% nominal volume fraction; and (c) 60% nominal volume fraction.

effects of structural heterogeneity on the permeability and on void formation. The permeability of the arrays of fiber bundles more closely resembled the permeability of the arrays of solid 0.635 cm diameter rods than the permeability expected for homogeneous arrays of 0.07112 cm diameter fibers. This is to be expected since the permeability of each fiber bundle was on the order of 10^{-8} cm^2 while the permeability of the array of solid rods was on the order of 10^{-3} cm^2 (see table 3). Table 6 shows the permeability of the fiber bundle arrays and the permeability of the corresponding arrays of solid rods. The permeability of the arrays of fiber bundles was always higher than the permeability measured with the solid rods, as the increase in porosity leads one to expect. Additionally, the measured permeability rose as the tow volume fraction, T_{vf}, of the fiber bundle fell.

The increase in the permeability of the arrays of fiber bundles, relative to the permeability of the solid rods, is not easily predictable with current models. For example, table 7 compares the experimental results with theoretical permeability predictions using several measures of the fiber volume fraction. The permeability prediction based on the tow volume fraction $K_{T_{vf}}$ is much too low because the tow volume fraction is larger than the nominal volume fraction and the fiber radius is much smaller than the tow radius. The permeability prediction based on the global volume fraction $K_{G_{vf}}$ is also too low because the small fiber radius dominates the calculation even though

Table 5. Comparison of the apparent shear index in the porous media to the value of n found by rheological characterization

N_{vf}, (%)	Apparent n in porous media	n from characterization
40	0.46	0.44
50	0.46	0.39–0.54
60	0.41	0.40

Table 6. Permeability of porous and solid rod fiber beds

Number of fibers in a bundle, N	N_{vf} (%)	G_{vf} (%)	T_{vf} (%)	K_s solid	K_p fiber bundle
50	40	26.4	62.7	3.97×10^{-3}	4.97×10^{-3}
55	40	29.1	69.0	3.97×10^{-3}	4.76×10^{-3}
60	50	38.4	75.3	1.23×10^{-3}	1.28×10^{-3}

the global volume fraction is smaller than the nominal volume fraction. Even the permeability prediction based on the effective cylindrical volume fraction $K_{C_{vf}}$ is not accurate, although in this case the prediction is too high. It is clear that none of these parameters offers a satisfactory way to predict the permeability of a heterogeneous media that consists of two embedded porous media of widely differing permeabilities and length scales.

An approximation of K_p for the arrays of fiber bundles may be generated based on the permeability K_s of the homogeneous array of solid rods at the nominal fiber volume fraction. However, as the tows are porous and contain fibers, one needs to scale the prediction of permeability with the tow volume fraction, T_{vf}, and the maximum volume fraction, v_{fmax}. At v_{fmax}, the permeability of the tow will approach zero and the permeability of the heterogeneous media of fiber bundles will correspond to the permeability of a homogeneous media of solid rods at the same nominal volume fraction. We then assume that K_p can be related to K_s by a series expansion in which a function of the tow volume fraction is the expansion parameter

$$K_p = K_s \sum_{n=0}^{\infty} k_n \left\{ 1 - \frac{T_{vf}}{v_{fmax}} \right\}^n = K_s[k_0 + k_1 x + k_2 x^2 + \cdots] \quad [14]$$

and $x = 1 - (T_{vf}/v_{fmax})$. Clearly, k_0 must be unity since $K_p = K_s$ if $x = 0$ ($T_{vf} = v_{fmax}$). For the large values of T_{vf} used in the current work, x is small, and the linear term in the expansion may suffice to approximate the experimental results. If the packing arrangement of fibers in the tow is assumed to be a square array, the maximum allowable value of tow volume fraction is $v_{fmax} \approx 78\%$, and if the packing arrangement is assumed to be hexagonal, $v_{fmax} \approx 91\%$. Figure 6 illustrates the usage of [14] by plotting the experimental values of K_p/K_s as a function of x for two cases, the case where x is computed assuming a square packing array and the case where x is computed assuming a hexagonal packing array of fibers in the tows. In the case of the square array, a linear least squares fit of all four data points (circular symbols) provides an accurate fit

$$\frac{K_p}{K_s} = 1.006 + 1.358 \cdot x \quad [15]$$

as shown by the solid line in figure 6 and by the numerical values provided in table 8. In the case of the hexagonal array, a fit to all four data points (triangular symbols) is clearly inaccurate

$$\frac{K_p}{K_s} = 0.973 + 0.829 \cdot x \quad [16]$$

First, the line does not fit the points closely, especially the point located at $x = 0.173$. Second, the y intercept which corresponds to k_0 in [14] is not very close to unity. Thus, the correlation with [14] indicates that the expected fiber arrangement within the model tows is a square array.

The packing arrangement of the nylon fibers within the model tows is illustrated in figure 7(a), and shows regions of both square and partly hexagonal packing. The square packed regions in the model tows may have dominated the flow behavior, however, errors in the experimental

Table 7. Experimental and theoretical permeabilities of fiber bundle beds

K_p fiber bundle	T_{vf} (%)	Theoretical $K_{T_{vf}}$	G_{vf} (%)	Theoretical $K_{G_{vf}}$	C_{vf} (%)	Theoretical $K_{C_{vf}}$
1.28E − 3	75.3	2.50×10^{-7}	38.4	5.63×10^{-5}	37.6	3.64×10^{-3}
4.76E − 3	69.0	1.12×10^{-6}	29.1	1.47×10^{-4}	27.6	9.44×10^{-3}
4.97E − 3	62.7	3.57×10^{-6}	26.4	1.97×10^{-4}	25.1	1.12×10^{-2}

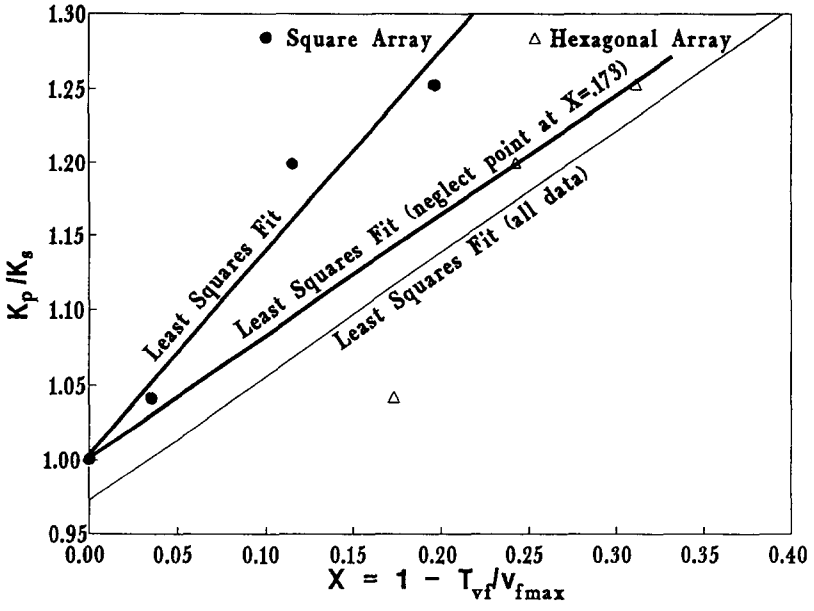

Figure 6. The experimental measurements of permeability in the porous bundles plotted according to [14], assuming either a square packing or a hexagonal packing arrangement of the fibers in the fiber bundle.

measurements may also have contributed to the better fit in the correlation for the square packing than for the hexagonal packing. For example, if the experimental point with $K_p/K_s = 1.041$ is in error, and a linear fit is done on the remaining three points, the resulting fits show very close correlation with the points computed assuming a hexagonal array rather than the square array, as illustrated in figure 6 by the line labeled "least squares fit (neglect point at $X = 0.173$)". However, the data were taken very carefully, figure 6 indicates that the flow behavior was probably governed by the regions of square packed fibers, and figure 7(a) shows a predominance of square or partially square packed regions. In any case, more data would clearly be helpful in discerning the flow behavior in heterogeneous porous media. This study indicates that despite the construction of a model porous media uncertainty persists concerning the exact microstructure. Unlike fibrous reinforcements, however, this uncertainty can be resolved by using more careful construction techniques when building model porous media in the future.

From these results it is clear that [14] gives an acceptable approximation for flow in heterogeneous porous media despite the uncertainties in the experimental measurements. Although closer agreement with the experimental data could have been obtained in the case of square packing by using a non-zero value of k_2, there is insufficient data to justify a non-linear model approximation. However, a more sophisticated model is clearly required because [14] does not work correctly in the limit of high values of the nominal fiber volume fraction N_{vf}. As N_{vf} approaches 78%, the maximum packing fraction, K_s approaches zero since flow could not occur through such a bed of solid fibers. The permeability of a bed of porous fibers would not be zero in such a case. Nevertheless, [14] may offer a simple but acceptable model for many practical applications.

Table 8. Comparison of experimental permeability enhancement K_p/K_s to predicted values using [14], assuming either square or hexagonal packing

T_{vf} (%)	Experimental K_p/K_s	Predicted K_p/K_s square array, [15]	Percent difference	Predicted K_p/K_s, hexagonal array [16]	Percent difference
62.7	1.252	1.272	1.6	1.230	−1.8
69.0	1.199	1.162	−3.1	1.173	−2.2
75.3	1.041	1.054	1.2	1.116	7.2
100 (solid)	1.0	1.006	0.6	0.973	−2.7

The effect of structural heterogeneity on the unsaturated flow is, perhaps, more important than the effect on the permeability, or saturated flow. The previous microflow model summarized above (see [8]–[11]), and the experimental work of Haywood & Harris (1990), has shown that voids may be expected to form at the flow front during liquid molding. The flow experiments with the model porous media constructed of fiber bundles provided an opportunity to test the air entrapment hypothesis of the microflow model (Parnas & Phelan 1991) and to observe the flow behavior in a well specified geometry. However, the experiments did not generate large enough pressure gradients to perform a quantitative test of the fiber bundle infiltration dynamics predicted by the microflow model.

The behavior at the flow front followed the pattern depicted in figure 7(b)–(d) in each experiment conducted with the fiber bundles. As the fluid flow met the fiber bundles, air was trapped in the fiber bundles. The flow front could clearly be seen to approach the fiber bundle, impregnate a fiber or two into the bundle while flowing around, and finally combining above the fiber bundle. As the flow progressed through the mold, the air remained trapped in the fiber bundles, forming voids. A higher tow volume fraction, T_{vf}, led to less fluid penetration of the bundle. After the flow front passed a fiber bundle creating a void, the void size did not remain constant, but slowly became smaller as the flow progressed through the mold. Both the pressure increase in the fluid outside the bundle and capillary action within the bundle could lead to void size reduction over time. These two effects could not be quantitatively distinguished in the tests conducted to date. However, it is worth noting that after the fluid filled the mold, and while the fluid continued to flow, the voids ceased shrinking, indicating that the increase in external bundle pressure as the mold initially filled probably caused the void shrinkage.

The tests were conducted at a variety of injection velocities and fluid viscosities, thereby varying the Reynolds number from 10^{-3} to 0.5, a range that includes many typical liquid molding processes. The other important parameter, the Capillary number, was not varied significantly due to difficulty in constructing the model porous media with fiber bundles. The capillary pressure in this work was probably much lower than in composite fabrication processes due to the large size of the fibers

(a)

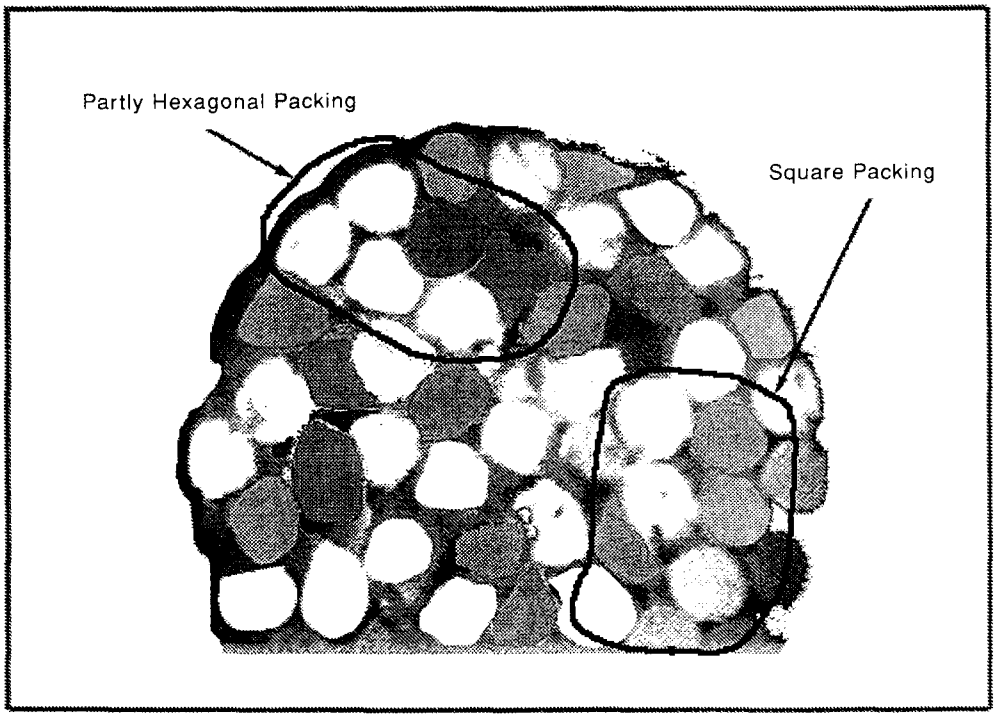

Figure 7(a). *Caption on p. 772.*

(b)

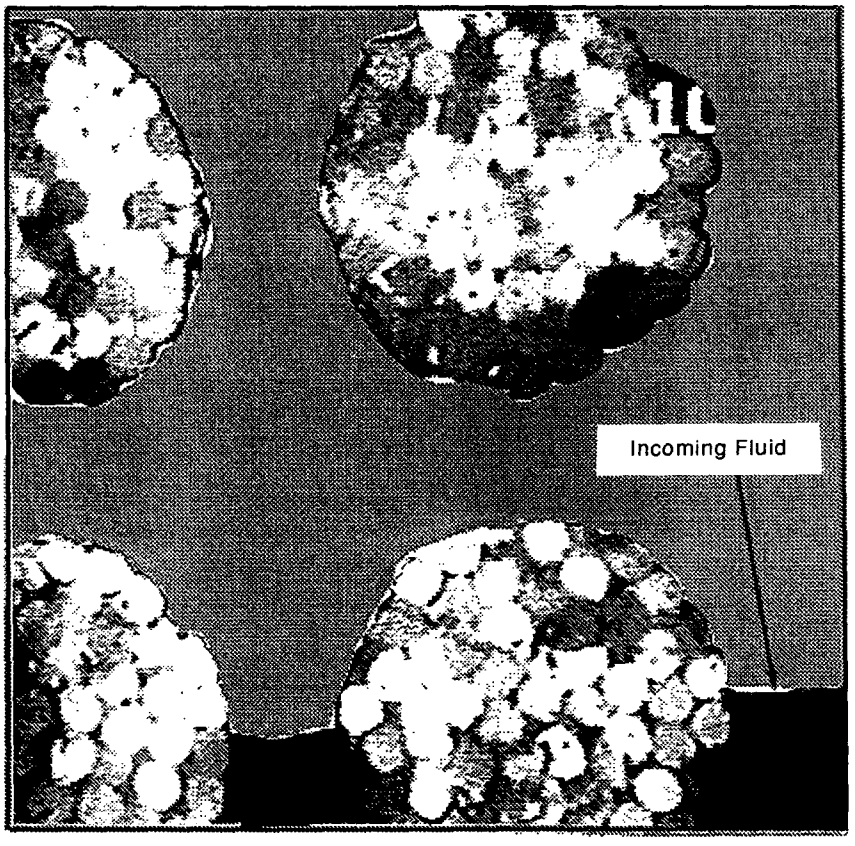

(c)

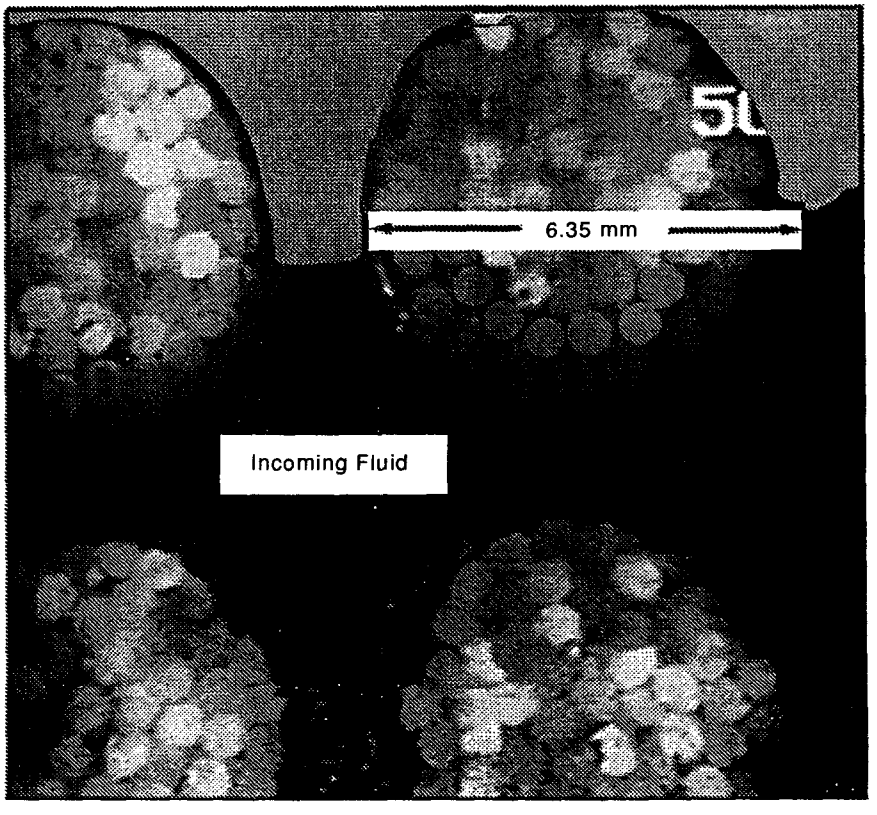

Figure 7(b) and (c). *Caption overleaf.*

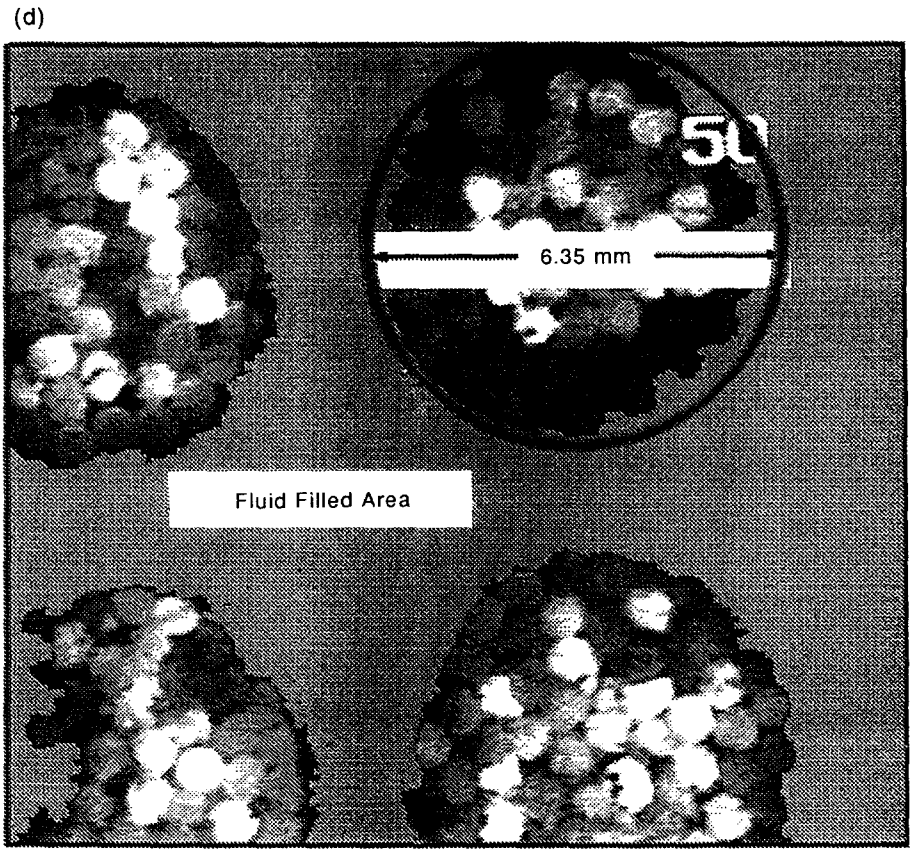

Figure 7(d).

Figure 7. Typical flow front behavior observed with fiber bundles. (a) The structure of a fiber bundle; (b) the flow front 3 s after fluid appeared at the bottom of the viewing window; (c) the flow front 13 s after fluid appeared; and (d) the fluid and trapped voids long after (45 s) the flow front passed out of the top of the viewing window.

used in the fiber bundles (~ 0.07 cm), relative to the fiber size in typical reinforcements (< 0.001 cm). The size of the fibers is important since the characteristic length scale of the interstitial flow spaces enters the definition of the capillary pressure, $\Delta p_c = (2\sigma \cos \theta)/r_i$, where σ is the fluid surface tension, θ is the contact angle and r_i is the characteristic size of the interstitial flow channels. Nevertheless, the similarity between the void formation seen at the flow front in this work and that seen previously with glass reinforcements (Haywood & Harris 1990) supports the hypothesis that structural heterogeneity leads to flow induced void formation.

The initial formation of the voids in the model tows appears to have occurred because the structure of the model tows was very dense compared to the average density of the porous media, forcing the fluid to flow preferentially around the model tow as depicted in figure 7. This heterogeneity in the model porous media may be characterized by comparing the overall porosity of the porous media, 61.6–73.6%, to the porosity within the model tows, 24.7–37.3% (see table 1). The heterogeneity in porosity is reflected in a heterogeneity in permeability. The measured permeability of the model porous media was, in one case, 3.97×10^{-3} cm^2, which is approximately six orders of magnitude larger than the estimated permeability of the model tows used in that experiment, 5.32×10^{-9} cm^2. The overall permeability was measured after the mold was filled and the permeability of the model tows was estimated with the asymptotic model discussed above. Although further refinements in the void formation experiment are necessary to properly scale all the relevant dimensionless groups simultaneously, the current experiments indicate that the air entrapment mechanism assumed in the model is reasonable. The fluid flow bypasses the fiber bundles much more rapidly than it penetrates them.

5. CONCLUSIONS

Excellent agreement was found between the measured permeability and the permeability predicted from the asymptotic model (Bruschke & Advani 1992) for Newtonian fluids flowing transversely to homogeneous arrays of rods. This agreement exists for fibers of two different radii and nominal volume fractions ranging from 40 to 60%. The dimensionless expression of K/R_f^2 was constant for different fiber radii with the same volume fraction. Therefore, the asymptotic model was an accurate predictor of the permeability for flow transverse to homogeneous beds of aligned fibers.

The measured permeability of heterogeneous arrays of fiber bundles was found to be up to 25% higher than the measured permeability of the corresponding homogeneous arrays of solid rods. The asymptotic model, or other models designed to predict the permeability of homogeneous porous media, cannot predict the permeability of the heterogeneous porous media, and attempts at prediction may produce errors in excess of an order of magnitude. This means that processing variables and predictions based on a measured global volume fraction will not be correct for the actual situation. A simple approximation based on the permeability computed at the nominal volume fraction, N_{vf}, and scaled by the tow volume fraction, T_{vf}, gives excellent agreement with the measured permeabilities of the arrays of fiber bundles, but needs extensive verification.

The experiments with the fiber bundles also provided an opportunity to observe the flow behavior at the flow front. Flow induced void formation in the fiber bundles was observed, in support of the hypotheses used in the model of Parnas & Phelan (1991). A void formed in a fiber bundle when the flow front met a fiber bundle and encompassed it, and the voids remained stable afterwards. Lower volume fractions inside the tows produced smaller voids, as well as higher permeabilities. The transient nature of the flow front behavior has been modeled, and the model connects the microscopic behavior at the flow front to many observed anomalies in the macroscopic flow such as the difference between "unsaturated" and "saturated" permeability. The support for the void formation mechanism assumed in the micro-flow model provided by the fiber bundle experiments gives greater weight to the results generated by such models.

The flow mobility of a strongly shear thinning fluid was measured in homogeneous arrays of rods and compared to the extended form of the asymptotic model. Although the differences between the model and experiment were as high as 30%, compared to differences of less than 10% for the case of a Newtonian fluid, such differences are probably reasonable in light of the additional experimental errors expected in the case of the shear thinning fluid. Once such experimental uncertainties are controlled, experiments in heterogeneous media with shear thinning fluids should prove useful for understanding power-law flow in realistic composite reinforcement geometries.

REFERENCES

Advani, S. G., Bruschke, M. V. & Parnas, R. 1994 *Flow and Rheology in Polymeric Composites Manufacturing* (Edited by Advani, S. G.), Chap. 12, pp. 465–516. Elsevier, Amsterdam.

Agarwal, B. D. & Broutman, L. J. 1980 *Analysis and Performance of Fiber Composites*. Wiley, New York.

Åström, B. T., Pipes, R. B. & Advani, S. G. 1992 On flow through aligned beds and its application to composites processing. *J. Composite Mater.* **20,** 1351–1373.

Broutman, L. J. & Krock, R. H. 1967 *Modern Composite Materials*. Addison–Wesley, Reading, MA.

Brown, R. C. 1984 A many fiber model of airflow through a fibrous filter. *J. Aerosol Sci.* **15,** 583–593.

Bruschke, M. V. 1992 A predictive model for permeability and non-isothermal flow of viscous and shear-thinning fluids in anisotropic fibrous media. Ph.D. thesis, University of Delaware, Newark, U.S.A.

Bruschke, M. V. & Advani, S. G. 1992 Flow of generalized Newtonian fluids across a periodic array of cylinders. *J. Rheol.* **37,** 479–498.

Carman, P. C. 1937 Fluid flow through granular beds. *Trans. Inst. Chem. Engrs* **15,** 150–166.

Chmielewski, C., Petty, C. A. & Jayaraman, K. 1990 Crossflow permeation of viscous and viscoelastic liquids in cylinder arrays. *Proc. Am. Soc. for Composites, Fifth Technical Conf.*, pp. 557–565.

Darcy, H. 1856 *Les Fonataines Publiques de la Ville de Dijon.* Dalmont, Paris.

Gebart, B. R. 1990 Permeability of unidirectional preforms for RTM. SICOMP Technical Report 90006.

Grove, R. A. 1980 Failure causes. In *Engineered Materials Handbook, Vol. 1, Composites.* ASM International, Metals Park, OH.

Gutowski, T. G., Cai, Z., Bauer, S., Boucher, D., Kingery, J. & Wineman, S. 1987 Consolidation experiments for laminate composites. *J. Composite Mater.* **21,** 650–669.

Haywood, A. & Harris, C. 1990 The effect of vacuum assistance in resin transfer moulding. *Composites Manufac.* **1,** 161–166.

Johnson, C. F. 1987 *Engineered Materials Handbook, Vol. 1, Composites*, pp. 564–568. ASM International, Metal Park, OH.

Kozeny, J. 1927 Uber kapillare Leitung des Wassers im Boden. *Sitz. Akad. Wissensh.* **136,** 271–306.

Lam, R. C. & Kardos, J. L. 1989 The permeability and compressibility of aligned and cross-plied carbon fiber beds during processing of composites. ANTEC '89, pp. 1408–1412.

Parnas, R. S. & Cohen, Y. 1987 Coupled parallel flows of power-law fluids in a channel and bounding porous medium. *Chem. Engng Commun.* **53,** 3.

Parnas, R. S. & Phelan, F. R. 1991 The effects of heterogeneous porous media on mold filling in resin transfer molding. *SAMPE Q.* 53–60.

Parnas, R. S. & Salem, A. J. 1993 A comparison of the unidirectional and radial in-plane flow of fluids through woven composite reinforcements. *Polym. Composites* **14,** 383.

Parnas, R. S., Salem, A. J., Sadiq, T. A. K., Wang, H. P. & Advani, S. G. 1994 The interaction between micro- and macroscopic flow in RTM preforms. *Composite Struct.* **27,** 93–107.

Sadiq, T., Parnas, R. & Advani, S. G. 1992 Experimental investigation of flow in resin transfer molding. *SAMPE Proc.* **24,** 660–674.

Sangani, A. S. & Acrivos, A. 1982 Slow flow through a periodic array of spheres. *Int. J. Multiphase Flow* **8,** 343–360.

Skartsis, L. & Kardos, J. L. 1990 The Newtonian permeability and consolidation of oriented carbon fiber beds. *Proc. Am. Soc. for Composites, Fifth Technical Conference.*

Skartsis, L., Khomami, B. & Kardos, J. L. 1992 Polymer flow through fibrous media. *J. Rheol.* **36,** 589–620.

Williams, J. G., Morris, C. E. M. & Ennis, B. C. 1974 Liquid flow through aligned fiber beds. *Polym. Engng Sci.* **14,** 413–419.